Macromolecular Research, Vol. 15, No. 5, pp 396-402 (2007)

Various Pattern-Forming States of Nematic Liquid Crystal Based on the Sign Inversion of Dielectric Anisotropy

Shin-Woong Kang* and Liang-Chy Chien

Liquid Crystal Institute and Chemical Physics Interdisciplinary Program, Kent State University, Kent, Ohio 44242, USA

Received January 8, 2007; Revised April 5, 2007

Abstract: The dielectric properties and various pattern-forming states of dual-frequency material in a nematic phase, as well as its mixture containing low concentrations of reactive monomers, are reported. The dielectric relaxation behaviors of nematic MLC 2048 are presented and compared to its mixture containing both mesogenic and nonmesogenic reactive monomers. The sign-inversion frequency of the dielectric anisotropy was significantly shifted on the addition of small amounts of the reactive monomers. However, all three mixtures used in this study essentially exhibited the same field-induced instabilities at different frequencies and voltage domains of the applied electric field. A broad band of modulated states were found to exist above a critical voltage and within a voltage-dependent frequency band in the vicinity of the sign-inversion frequency, f_i, of the dielectric anisotropy. As the f_i of the mixtures shifted, so did the bands of the modulated state of the different mixtures and the temperatures, which were well matched with the measured f_i value.

Keywords: liquid crystal, sign inversion of dielectric anisotropy, pattern formation, dual frequency.

Introduction

Various pattern-forming states of liquid crystals (LC) based on the director modulation due to either electrohydrodynamic or static dielectric effects under applied electric/magnetic fields are fascinating object for both fundamental science and applications.[1-6] The periodic director modulation combined by the electrically controllable director orientation of LC molecules leads to a realization of switchable optical diffraction gratings.[3,4] On the other hand, polymerization of various reactive monomers in the pattern-forming states as a reaction template resulted in the patterned phase separation, where the polymer networks are precisely replicated by the both orientational and spatial ordering of host LC molecules.[5,6]

In homogeneously aligned liquid crystal, two principal dielectric constants - $\varepsilon_{\parallel}$ parallel and $\varepsilon_{\perp}$ perpendicular to the molecular axis - can be measured. Both $\varepsilon_{\parallel}$ and $\varepsilon_{\perp}$ show a normal Debye-type of relaxation at microwave frequencies.[7] If the molecule has a permanent dipole incorporated along its long axis, the $\varepsilon_{\parallel}$ has an additional dispersion at very unusually low frequencies in the radio region.[8] The difference in relaxation behavior of $\varepsilon_{\parallel}$ and $\varepsilon_{\perp}$ is originated from the molecular structure and dynamic behavior. The dipole reorientation accomplished by a rotation around the long molecular axis is essentially not hindered by the nematic order. For $\varepsilon_{\perp}$, this is the main contribution to the relaxation process, which is not influenced by nematic potential. For the field along the director ($\varepsilon_{\parallel}$), a reorientation of the dipole is accompanied by the rotation of a molecule along its transverse axis, which is counteracted by the nematic potential.[7,8] Thus the molecule with a permanent dipole along its long axis shows additional relaxation process at low frequency region. In this case, for the molecule with a positive dielectric anisotropy ($\Delta\varepsilon > 0$) at very low frequency (or static state), the sign inversion process of $\Delta\varepsilon$ occurs at the frequency region of a dipole relaxation concerning $\varepsilon_{\parallel}$.[8-10] This type of material is denoted as a dual frequency nematic liquid crystal (DFNLC), which means the sign inversion of $\Delta\varepsilon$ at two different frequency domains.

In this article, we report various pattern-forming states of nematic LC based on the sign inversion of dielectric anisotropy. Dielectric relaxation behaviors of commercial nematic LC (MLC 2048) and its mixture with both mesogenic and nonmesogenic reactive monomers are carefully examined. We also summarize the optical states and transitional phenomena of these pattern-forming states together with the phase diagram, obtained by varying frequency and amplitude of applied electric field.

Experimental

A DFNLC and its mixtures with reactive monomers are prepared as the ratio of (a) 100% MLC 2048 (commercial

*Corresponding Author. E-mail: skang1@kent.edu

eutectic mixture, Merck), (b) MLC 2048/RM 257 = 95.0/5.0, and (c) MLC 2048/HDDA = 95.0/5.0 by weight, where the RM 257 (1,4-bis[3-(acryloyloxy)propyloxy]-2-methyl benzene, BDH) is mesogenic (i.e., liquid crystalline) monomer and HDDA (1,6-hexanediol diacrylate, Aldrich) is nonmesogenic monomer, respectively. Each mixture was injected into planar and homeotropic cells with well defined electrode area and thickness of LC layer. The LC alignment of the samples was confirmed with a polarized optical microscope.

The capacitance of each cell was measured using a LCR meter (HP4284A) at different temperature and frequency of an applied electric field. A sinusoidal waveform with amplitude of 0.5 V was used and the frequency was varied from 0.1 kHz to 1 MHz. The two principal dielectric constants ($\varepsilon_{\parallel}$ and $\varepsilon_{\perp}$) were calculated from the measured capacitance, electrode area, and sample thickness using the relation of $\varepsilon = Cd/\varepsilon_o A$, where ε_o, d, and A are the dielectric permittivity of vacuum, layer thickness, and area of electrode, respectively.[7] The capacitance values determined from homeotropic and homogeneous cells were used for $\varepsilon_{\parallel}$ and $\varepsilon_{\perp}$, respectively.

To study a wide range of field-induced optical patterns due to the periodic modulation of LC director, the DFNLCs are filled into both wedge-shaped and flat standard electro-optic cells with different cell gaps. A square waveform electric field at different amplitude and frequency is applied to the samples to induce a periodic modulation of director in the plane normal to the electric field. The various pattern-forming states are observed using a polarized optical microscope (Nikon OPTIPHOT2-POL) equipped with a temperature controller (Mettler FP52 Hot Stage). Based on the optical textures and diffraction patterns, the phase diagram is established from the frequency and amplitude of an applied field at constant temperature.

Results and Discussion

Figure 1 shows a dielectric relaxation behavior of a 100% MLC 2048 measured at different temperatures. The relaxation of the $\varepsilon_{\parallel}$ starts from much lower frequency (~10^4 Hz) than that of $\varepsilon_{\perp}$ (10^5~10^6 Hz). The relaxation of the $\varepsilon_{\parallel}$ exhibits an additional dispersion, which is clearly observed at low temperature. At 20 °C, the relaxation of a permanent dipole parallel to the molecular axis begins at the frequency $f < 10^4$ Hz and followed by the other relaxation, which occurs at the frequency f~10^5 Hz. These separate dispersions are gradually merged into the single relaxation process at higher temperatures. However, the relaxation of the $\varepsilon_{\perp}$ shows a monotonous dispersion at all measured temperatures. The values of dielectric constants for both $\varepsilon_{\parallel}$ and $\varepsilon_{\perp}$ show a minor decrease with the increase in temperature, except the dispersion region. More importantly, the relaxation frequency of the $\varepsilon_{\parallel}$ dramatically shifts toward higher frequency

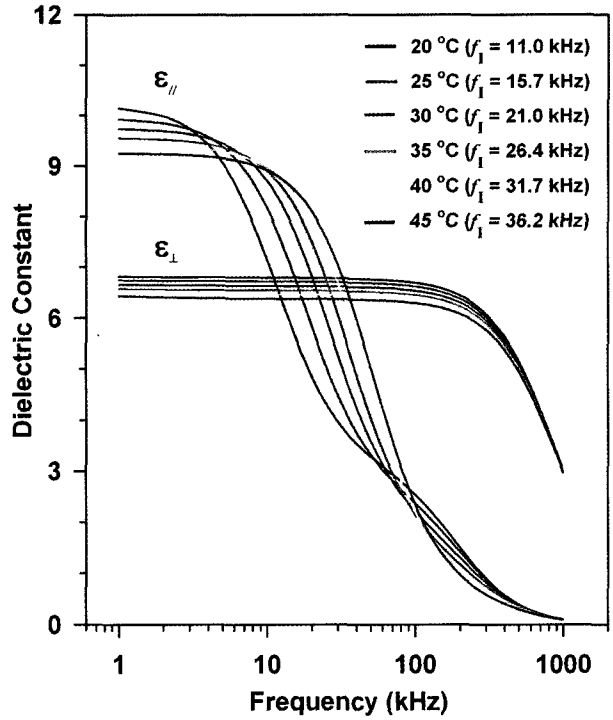

Figure 1. Dielectric relaxation of pure MLC 2048. The frequency dependence of dielectric constants ($\varepsilon_{\parallel}$ and $\varepsilon_{\perp}$) is shown for different temperatures: 20 °C (blue), 25 °C (red), 30 °C (green), 35 °C (pink), 40 °C (cyan), and 45 °C (dark red). The sign-inversion frequencies f_i of dielectric anisotropy are shown in the legend.

region with the temperature increase. This is due to the decrease in both rotational viscosity and nematic potential, which are counteracting to the dipole reorientation.[7] As a result, the crossover frequency for the sign inversion of dielectric anisotropy ($\Delta\varepsilon = \varepsilon_{\parallel} - \varepsilon_{\perp}$) increases with temperature.

For this type of dual-frequency LC materials, three frequency regimes exist for different behaviors with the change in temperature: (1) low frequency regime for $\Delta\varepsilon > 0$ at any temperature up to the T_{NI}, (2) high frequency regime for $\Delta\varepsilon < 0$ at all temperatures in nematic phase, and (3) relaxation frequency regime for the sign inversion of $\Delta\varepsilon$ with temperature change. Figure 2 displays a temperature dependence of dielectric constants at different frequency regimes. For both high and low frequency regimes, the measured dielectric permittivities (both $\varepsilon_{\parallel}$ and $\varepsilon_{\perp}$) decrease with temperature but no crossover is observed (Figure 2(a)). As expected for the relaxation frequency regime, the crossover between the two principal permittivities measured at 35 kHz is observed at 40 °C as shown in Figure 2(b).

The effects of temperature dependence of dielectric relaxation are observed for the mixtures with 5 wt% RM 257 or 5 wt% HDDA in MLC 2048. Although the differences in $\varepsilon_{\perp}$ are not observed, the relaxation frequency for $\varepsilon_{\parallel}$ is signifi-

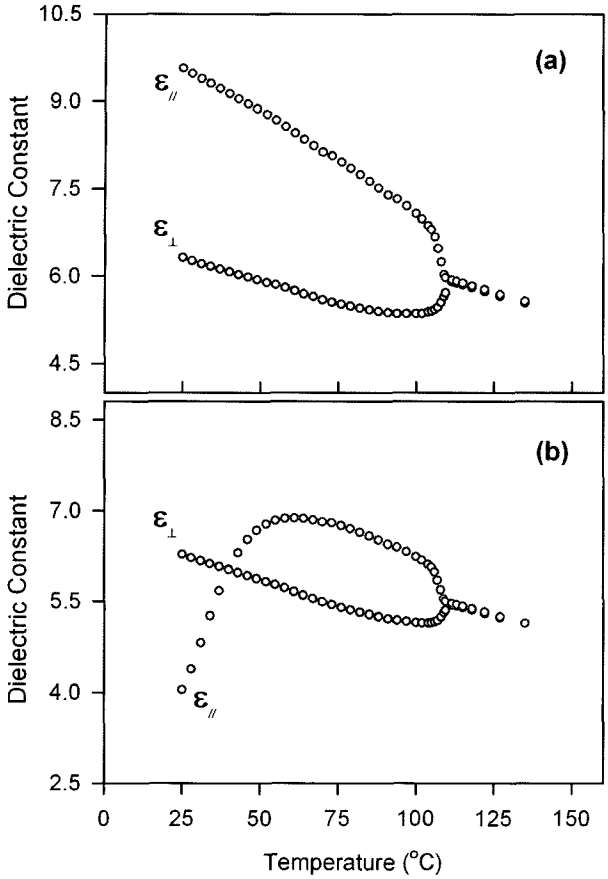

Figure 2. Temperature dependence of dielectric constants at two different frequency regimes for 100% MLC 2048: (a) At 1 kHz, low frequency regime for $\Delta\varepsilon > 0$ and (b) at 35 kHz, relaxation frequency regime for sign inversion of $\Delta\varepsilon$.

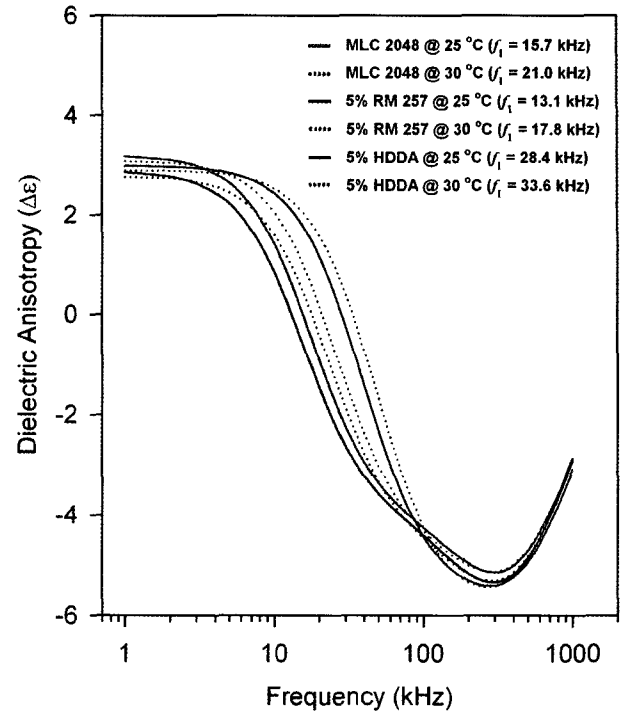

Figure 3. Material dependence of the sign inversion frequency of $\Delta\varepsilon$. By adding a small amount of a reactive monomer, the sign inversion frequency shifts depending on the type of monomer for both temperatures (25 °C and 30 °C). Addition of 5 wt% mesogenic monomer RM 257 results in a shift toward lower frequency (-2.6 kHz at 25 °C and -3.2 kHz at 30 °C). The same amount of nonmesogenic monomer HDDA induces a shift toward higher frequency (+12.7 kHz at 25 °C and +12.6 kHz at 30 °C). The sign-inversion frequencies of dielectric anisotropy are presented in the legend.

cantly modified by adding a small amount of reactive monomer. As shown in Figure 3, the sign inversion frequency f_I for the mixture with a RM 257 is slightly shifted to lower frequency (-2.6 kHz shift at 25 °C). For the mixture with 5% HDDA in MLC 2048, the sign-inversion frequency f_I is significantly shifted toward the higher frequency (+12.7 kHz shift at 25 °C). This phenomenon is presumably originated from the different dielectric properties of reactive monomers. The isotropy in molecular shape and dielectric relaxation of the HDDA give rise to more freedom for dipole reorientation (dilution effect). On the other hand, the mesogenic molecule RM 257 with $\Delta\varepsilon < 0$ decreases $\varepsilon_{\parallel}$ and increases $\varepsilon_{\perp}$ of the mixture, resulting in the lower crossover frequency f_I.

As seen in Figure 4, the sign-inversion frequency of pure MLC 2048 clearly increases by the increase in temperature. The temperature dependence of sign-inversion frequency of $\Delta\varepsilon$ for three LC mixtures used in the study is plotted in the inset of Figure 4. The measured sign-inversion frequency f_I is linearly increases for all three samples at the temperature range far away from the T_{NI} (106 °C for MLC 2048). However the increase starts level off and the sign-inversion frequency tends to saturate upon approaching the nematic to isotropic transition temperature.

In typical nematics confined with uniform director orientation between parallel flat substrates, a voltage $V > V_{th} \sim \sqrt{K/Re\Delta\varepsilon}$ applied across the substrates induces a Frederiks transition to a distorted state, which, however, remains uniform in the substrate plane. No in-plane modulation (or pattern-forming state) occurs. Here K is an elastic constant for deforming the equilibrium director orientation, and $Re\Delta\varepsilon$ is the real part of the dielectric anisotropy given as a function of frequency f by

$$Re\Delta\varepsilon(f) = \varepsilon_{\parallel}(\infty) - \varepsilon_{\perp}(\infty) + \frac{\varepsilon_{\parallel}(0) - \varepsilon_{\parallel}(\infty)}{1 + f^2/f_{\parallel}^2} + \frac{\varepsilon_{\perp}(\infty) - \varepsilon_{\perp}(0)}{1 + f^2/f_{\perp}^2},$$

where the subscripts $\parallel$, $\perp$ refer to the principal values of the dielectric constant and $f_{\perp}$, $f_{\parallel}$ are the lowest dipole relaxation frequencies.[11] In most nematics, $f_{\perp} \sim f_{\parallel} \sim 10^8$ Hz, so that $Re\Delta\varepsilon$ is essentially frequency independent for practical operating frequencies.

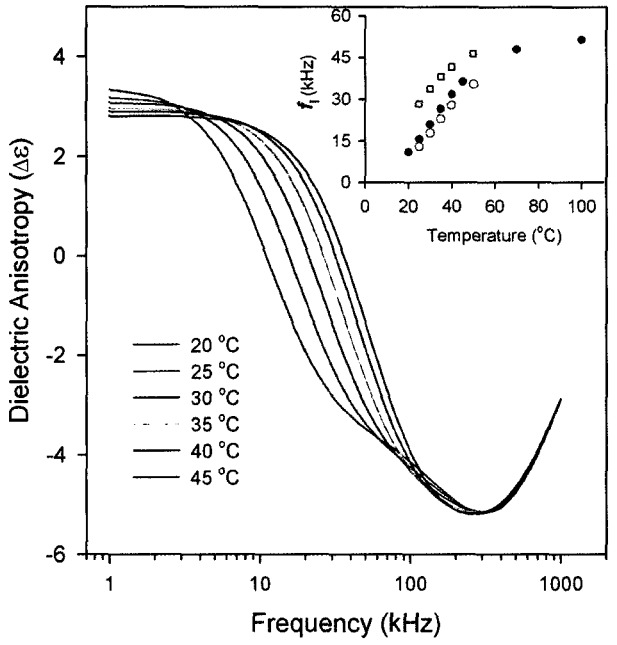

Figure 4. Temperature dependence of dielectric anisotropy ($\Delta\varepsilon$) of pure MLC 2048. (Inset): The sign-inversion frequency of all three mixtures shows a linear relationship at the temperature region far away from a nematic-isotropic transition. The f_l tends to saturate upon approaching the nematic to isotropic transition temperature (106°C). The filled circles, empty squares, and empty circles represent pure MLC 2048, 5 wt% HDDA, and 5 wt% RM 257 mixtures, respectively.

The pattern-forming state in one dimension was observed, first by de Jeu *et al.*,[12-14] using the material, ordinary Frederiks distortion diverges ($V_{th} \propto 1/\sqrt{Re\Delta\varepsilon} \rightarrow \infty$), and simple distortions with whose dielectric anisotropy changes sign at a specific inversion frequency f_l. In this and similar materials, $\varepsilon_{\parallel}(0) > \varepsilon_{\perp}(0) > \varepsilon_{\parallel}(\infty)$ and $f_{\parallel} \sim 10^4$ Hz $<< f_{\perp}$. The expression for $Re\Delta\varepsilon$ at low frequency then simplifies to

$$Re\Delta\varepsilon(f) = \varepsilon_{\parallel}(\infty) - \varepsilon_{\perp}(0) + \frac{\varepsilon_{\parallel}(0) - \varepsilon_{\parallel}(\infty)}{1 + f^2/f_{\parallel}^2},$$

and $Re\Delta\varepsilon$ passes through zero at

$$f_l = f_{\parallel}\left(\frac{\varepsilon_{\parallel}(0) - \varepsilon_{\perp}(0)}{\varepsilon_{\perp}(0) - \varepsilon_{\parallel}(\infty)}\right)^{1/2} \sim 10^4 \text{ Hz}.$$

Thus, when, $f \sim f_l$, the threshold voltage for the ordinary Frederiks distortion diverges ($V_{th} \propto 1/\sqrt{Re\Delta\varepsilon} \rightarrow \infty$), and simple distortions with $\theta = \theta(z)$ no longer occur. Instead, the dielectric contribution to the free energy is dominated by dielectric losses ($Im\Delta\varepsilon >> Re\Delta\varepsilon \cong 0$). As pointed out by Chigrinov and coworkers[15] (and in an alternative analysis as an electrohydrodynamic instability by de Jeu[12-14]), more complicated distortions with $\theta = \theta(x, z)$, corresponding to states that are modulated in the plane of the substrates, may be induced in the vicinity of f_l.

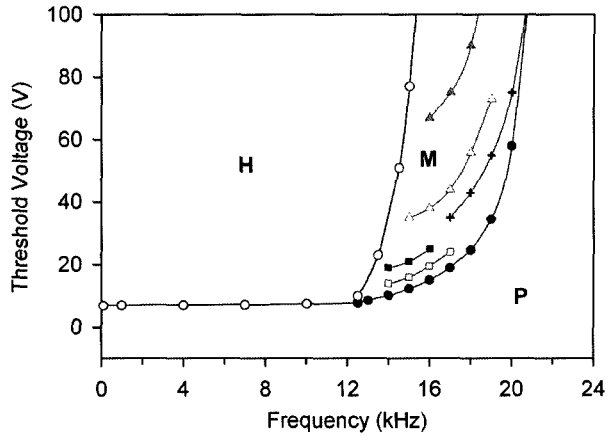

Figure 5. Phase diagram of the various pattern-forming states for pure MLC 2048 measured using 10.0 ± 0.5 μm sample at 25 °C. P and H denote uniform homogeneous and homeotropic states, respectively, whose phase boundaries are indicated by the lines connecting the filled and open circles. M denotes various states in which the director is spatially modulated in the plane of the substrates. Triangles and filled squares are lower limits in voltage for distinct two-dimensionally modulated states. The crosses indicate a lower limit for a chevron texture. Open squares and filled circles correspond to the threshold for the one-dimensional modulated states. The corresponding optical micrographs are presented in Figure 6.

All three DFNLC mixtures used in this study show essentially the same field-induced instabilities at different frequency and voltage domains of applied electric field. The broad band of the modulated states (denoted as M, surrounded by two diverging curves) exists above a critical voltage and within a voltage-dependent frequency band at the vicinity of the sign-inversion frequency f_l of dielectric anisotropy (Figure 5). On either side of this band is uniform states - planar aligned (P) and homeotropically aligned (H) states. As the f_l of the mixtures shifts, the bands of the modulated state for different mixtures and temperatures are also shifted and well matched with the measured value of f_l. The threshold frequency and voltage of each texture show a critical dependence on temperature and also the pattern formation exhibits much more hysteresis compared to the ordinary cholesteric LCs.

Figure 5 plots the various pattern-forming states and their threshold characteristics obtained from 100% MLC 2048 with a 10.5 ± 0.5 μm-thick cell at 25 °C. Figure 6 presents the corresponding optical textures of various pattern-forming states. At low frequencies (< 12 kHz), only the ordinary Fredericks-type transition ($\theta = \theta(z)$) from planar to homeotropic state appears at applied voltage of ~ 7 V_p (marked with open circles). This uniform transition state was also obtained from periodic pattern-forming states at even higher frequency (open circles above M state). The typical texture (Figure 6(a)) obtained during the transition shows shrinking

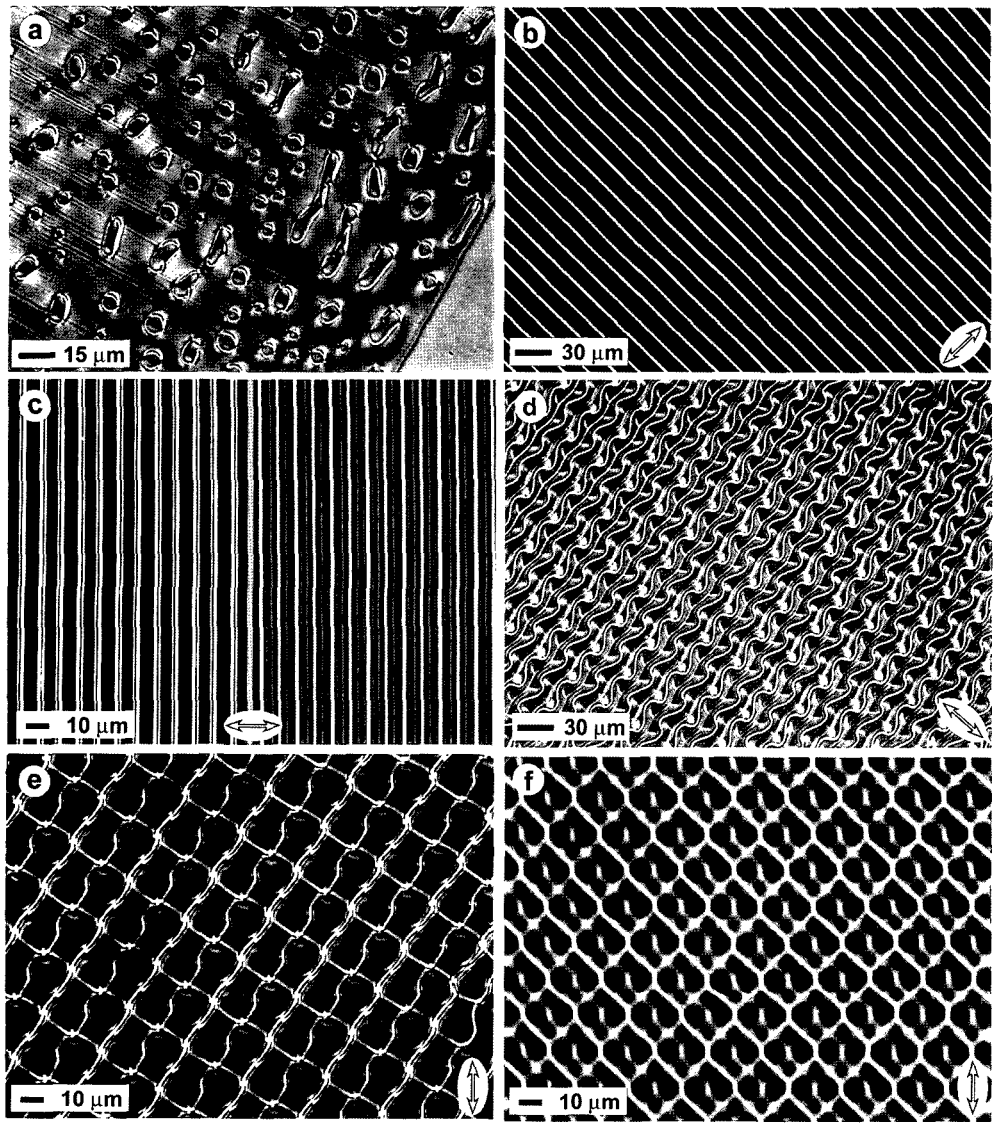

Figure 6. Optical images of pattern-forming states observed in the DFNLC (100% MLC 2048). Each image corresponds to the (a) looped-domains on uniform Fredericks state at $f = 11$ kHz, $V_p = 38$ V, and $d = 25$ μm, (b) the 1D-A texture at $f = 14$ kHz, $V_p = 10.2$ V, and $d = 10.5$ μm, (c) the 1D-B texture at $f = 15$ kHz, $V_p = 16$ V, and $d = 10.5$ μm, (d) the undulated stripe texture at $f = 16$ kHz, $V_p = 28$ V, and $d = 25$ μm. Polarizer is parallel to the image frame and analyzer is crossed for (a) ~ (d). Quarter wave-plate was placed at 45° to the polarizer and analyzer for (c) right panel, (e) the 2D-A texture at $f = 16$ kHz, $V_p = 39$ V, and $d = 25$ μm, and (f) the 2D-B textures at $f = 17$ kHz, $V_p = 78$ V, and $d = 25$ μm. Polarizer is parallel (e) and perpendicular (f) to the rubbing direction. No analyzer is used for (e) and (f). Arrows indicate surface rub-direction.

looped-domains on the uniformly tilted (reddish) background. The threshold voltage increases with the frequency and diverges when the frequency approaches to the f_l (i.e. $\Delta\varepsilon \rightarrow 0$). At the frequency near the f_l with $\Delta\varepsilon > 0$, the one-dimensional striped pattern, denoted by filled circle in Figure 5 (1D-A texture, Figure 6(b)), was induced from the uniform planar state P. Figure 6(b) shows the striped-domain structure with the 30-micron optical period observed from a 10 ± 0.5 μm sample cell. The domains are perpendicular to the rubbing direction with one optical period consisted of two bright lines with different intensity. The other couple of bright lines become visible when a quarter waveplate is placed at 45° with respect to the surface rub-direction (indicated by double-ended arrow). With a slight increase in applied voltage (open squares in Figure 5), this semi-static pattern becomes highly dynamic state, which stripes are swaying along its perpendicular direction. Further increase in applied voltage causes the stripes broken up into small pieces of looped-domain. The random movement of (looped) stripes results in a strong light scattering state. Interestingly,

these broken stripes very slowly reorganize at the same field condition and yield a similar pattern exhibiting uniform stripe domains perpendicular to the rubbing direction. As in the 1D-A state in Figure 6(b), the 1D-B texture exhibits two bright lines in one period when the rubbing direction is parallel to the polarizer and perpendicular to the analyzer (Figure 6(c), left panel). The additional sharp bright lines appear when a quarter waveplate is placed at 45° with respect to the surface rubbing direction (Figure 6(c), right panel). Although the optical texture looks similar, the director modulation of the 1D-B state seems to be much stronger than that of 1D-A. In contrast to the 1D-A texture, the 1D-B texture shows a strongly modulated and stable (or static) state, and its optical period is significantly different from the 1D-A (about one half of the 1D-A state).

Both the 1D-A and 1D-B patterns exhibit the similar transitional behavior. The pattern appears uniformly in a whole sample area at the threshold voltage without slow nucleation and propagation processes. The patterns show maximum diffraction efficiencies for the incident light polarized perpendicular to the stripe domains. This suggests that, as predicted for the modulated Fredericks distortion (the 1D-A and 1D-B states),[15] the director modulation in these states is primarily bend/spray distortion of the optical axis, with the wave vector parallel to the average director (i.e., the average director lies perpendicular to the stripe domain).

At higher voltage, the stripe domains shrink and yield loop domains on the uniform background as shown in Figure 6(a) (corresponding to the open circles above M state in Figure 5). The uniform texture ends up with a homeotropic state at sufficiently high voltage. This threshold voltage diverges at the $f=f_l$ (i.e., $V_{th} \propto 1/\sqrt{Re\Delta\varepsilon} \rightarrow \infty$).

On the other hand, the 1D-B texture transforms to the static undulated domains by the small increase of the voltage (filled squares in Figure 5) when the frequency is getting closer to f_l. As seen in Figure 6(d), two types of bright lines perpendicular to the surface rub direction alternate with a different degree of undulation. Another set of bright lines with weak intensity appears behind the undulated lines parallel to the rubbing direction, resulting in a two-dimensional periodic pattern. Above this voltage and frequency, the flowing domains (parallel to the undulated stripe) with 1D or 2D patterns appear and expand through the entire sample. At higher frequency ($f>f_l$), the 2D patterns become much more stable while the 1D textures are very unstable and highly dynamic. The optical textures of high voltage region ($>30V_p$) of the M state of the phase diagram show highly dynamic and hysteretic states. These textures include

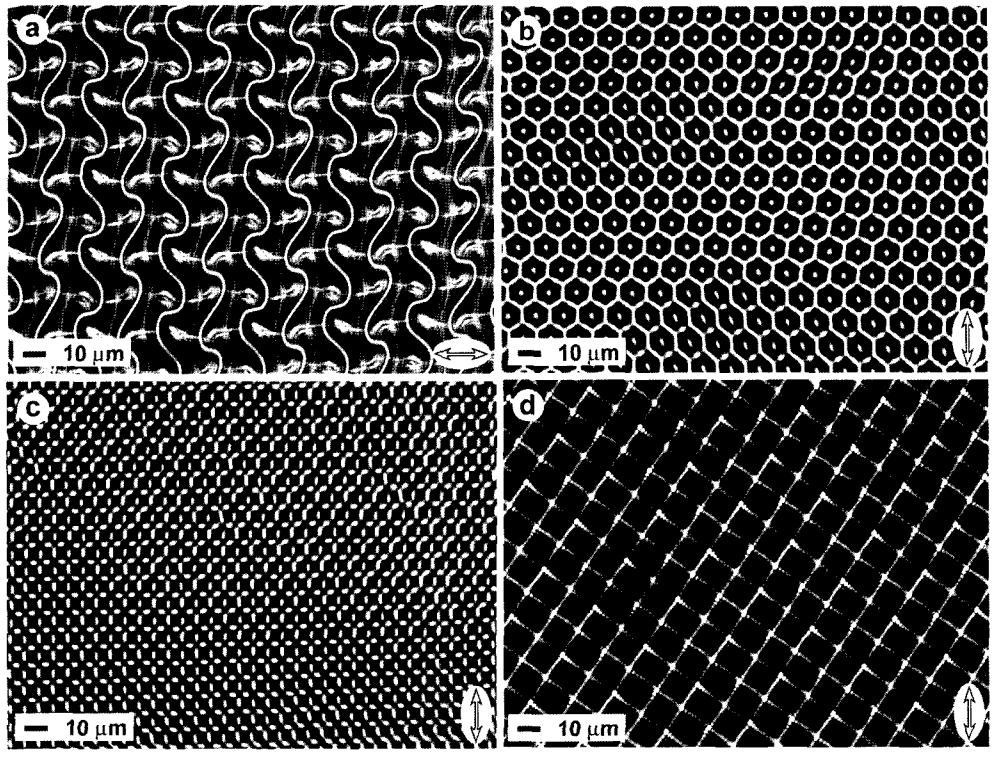

Figure 7. Optical micrographs of additional 2D-patterns observed from (a) 25 μm sample at $f=16$ kHz and $V_p=32$ V, (b) 25 μm sample at $f=18$ kHz and $V_p=79$ V, (c) 10.5 μm sample at $f=18$ kHz and $V_p=42$ V, and (d) 25 μm sample at $f=16$ kHz and $V_p=33$ V. Polarizer is perpendicular (c) and parallel (d) to the surface rubbing direction denoted by double-ended arrow. No analyzer is used. Polarizer is parallel (a ~ c) and perpendicular (d) to the horizontal image frame. No analyzer is used.

a chevron (cross), 2D-A (open triangle), 2D-B (filled triangle), and chaotic turbulence. The 2D-A (Figure 6(e)) and 2D-B (Figure 6(f)) exhibit similar patterns and phase behaviors but they are clearly separated by the strong turbulence. The chevron state and 1D-A pattern become very unstable and then indistinguishable at high frequency and voltage region (indicated by cross and filled circle). The additional 2D pattern-forming states are also observed for this region and their optical micrographs are presented in Figure 7. The undulated pattern shown in Figure 7(a) is obtained from the 25 μm sample at f = 16 kHz and V_p = 32 V. The hexagonal pattern (Figure 7(b)) and square-grid pattern (Figure 7(d), lattice vector tilted 45° to the rub direction) were also observed from the same sample at f = 18 kHz, V_p = 79 V and f = 16 kHz, V_p = 33 V, respectively. Another square-grid pattern (Figure 7(c), lattice vector parallel and perpendicular to the rub direction) was obtained from 10 ± 0.5 μm sample at f = 18 kHz and V_p = 42 V.

In general, the one-dimensional patterns are stable near the low frequency limit and become unstable at higher frequency (especially for $f > f_l$) countering to the 2D-patterns, which are stable at the frequency $f > f_l$ and disappear at the frequency $f < f_l$. It should be emphasized that the optical period of all modulated states observed in this type of material is strongly dependent on the sample thickness, frequency and voltage of applied electric field. The optical period is proportional to the sample thickness and applied voltage but inversely proportional to the frequency. During the transition, the textures appear instantly throughout the entire sample at a certain on-set voltage and frequency without slow nucleation and propagation processes.

We end this report with a comment on the origin of the pattern formation observed in our type of DFLC. De Jeu *et al.*[12-14] have proposed that the 1D-A and 1D-B states arise from electrohydrodynamic convection. However, Chigrinov *et al.*[15] more recently showed that both 1D (1D-A and 1D-B) and 2D (2D-A and 2D-B) patterns can be comprehensively explained by a single theory involving static distortions due to dielectric and elastic constants (rather than conductivity and viscosity). Hysteretic behavior of some of the pattern-forming states observed in our study could be attributed to either the electrohydrodynamic convection or temperature sensitivity of sign inversion frequency of $\Delta\varepsilon$. Therefore, to draw a clear conclusion a more detailed study is required including conductivity measurement during transition, observation of particle movement in the patterns, etc.

As we demonstrated above, nematic dual-frequency liquid crystal forms a variety of distinct pattern-forming states with the variation of frequency and amplitude of applied electric field. As the orientation of LC director is electrically controllable, these periodic optical states can be used for switchable diffraction gratings. Especially polymer stabilized textures, where the small amount of polymer network stabilizes the pattern-forming states against removal of electric field, can be used for practical applications. The diversity of optical patterns provides more opportunities to select proper optical diffracting states. In addition, based on the previous report[5,6] of templating polymer network in the cholesteric fingerprint texture, we believe that various patterns obtained from DFLC can also be used as a template. This expands the flexibility of templating functional polymers and particles by utilizing LC pattern-forming states.

References

(1) a) J. T. Gleeson, *Nature*, **385**, 511 (1997), b) A. Buka and L. Kramer, *Pattern Formation in Liquid Crystals*, Springer-Verlag, New York (1996).

(2) a) C. S. Cho, I. K. Park, J. W. Nah, and T. Akaike, *Macromol. Res.*, **11**, 2 (2003), b) S. W. Nam, S. H. Kang, and J. Y. Chang, *Macromol. Res.*, **15**, 74 (2007).

(3) D. Subacious, P. J. Bos, and O. D. Lavrentovich, *Appl. Phys. Lett.*, **71**, 1350 (1997).

(4) a) S. W. Kang, S. Sprunt, and L.C. Chien, *Appl. Phys. Lett.*, **76**, 3516 (2000). b) T. Kyu, S. Meng, H. Duran, K. Nanjundiah, and G. R. Yandek, *Macromol. Res.*, **14**, 155 (2006).

(5) S. W. Kang, S. Sprunt, and L. C. Chien, *Adv. Mater.*, **13**, 1179 (2001).

(6) S. W. Kang, S.-H. Jin, L. C. Chien, and S. Sprunt, *Adv. Func. Mater.*, **14**, 329 (2004).

(7) W. H. de Jeu, *Physical Properties of Liquid Crystalline Materials*, Gordon and Breach, Science Pubublishers, New York, 1980.

(8) G. Meier and A. Saupe, *Mol. Cryst.*, **1**, 515 (1966).

(9) W. H. de Jeu and T. W. Lathouwers, *Mol. Cryst. Liq. Cryst.*, **26**, 225 (1973).

(10) M. Schadt, *Mol. Cryst. Liq. Cryst.*, **66**, 319 (1981).

(11) L. M. Blinov and V. G. Chigrinov, *Electrooptic Effects in Liquid Crystal Materials*, Springer-Verlag, New York, 1994.

(12) (a) W. H. de Jeu, C. J. Gerristsma, and T. W. Lathouwers, *Chem. Phys. Lett.*, **14**, 503 (1972), (b) W. J. A. Goossens, *Phys. Lett.*, **40A**, 95 (1972).

(13) W. H. de Jeu, C. J. Gerristsma, P. V. Zanten, and W. J. A. Goossens, *Phys. Lett.*, **39A**, 355 (1972).

(14) W. H. de Jeu and T. W. Lathouwers, *Mol. Cryst. Liq. Cryst.*, **26**, 235 (1973).

(15) V. G. Chigrinov, T. V. Korkishko, M. I. Barnik, and A. N. Trufanov, *Mol. Cryst. Liq. Cryst.*, **129**, 285 (1985).